



**HAL**  
open science

## Ca<sup>++</sup> activated Cl<sup>-</sup> currents are dispensable for olfaction

Gwendolyn M Billig, Balazs Pal, Pawel Fidzinski, Thomas J Jentsch

► **To cite this version:**

Gwendolyn M Billig, Balazs Pal, Pawel Fidzinski, Thomas J Jentsch. Ca<sup>++</sup> activated Cl<sup>-</sup> currents are dispensable for olfaction. *Nature Neuroscience*, 2011, 10.1038/nn.2821 . hal-00634804

**HAL Id: hal-00634804**

**<https://hal.science/hal-00634804>**

Submitted on 24 Oct 2011

**HAL** is a multi-disciplinary open access archive for the deposit and dissemination of scientific research documents, whether they are published or not. The documents may come from teaching and research institutions in France or abroad, or from public or private research centers.

L'archive ouverte pluridisciplinaire **HAL**, est destinée au dépôt et à la diffusion de documents scientifiques de niveau recherche, publiés ou non, émanant des établissements d'enseignement et de recherche français ou étrangers, des laboratoires publics ou privés.

## **Ca<sup>++</sup>-activated Cl<sup>-</sup>-currents are dispensable for olfaction**

Gwendolyn M. Billig<sup>1,§</sup>, Balázs Pál<sup>1</sup>, Pawel Fidzinski<sup>1</sup> & Thomas J. Jentsch<sup>1,2,\*</sup>

<sup>1</sup>Leibniz-Institut für Molekulare Pharmakologie (FMP) / Max-Delbrück-Centrum für Molekulare Medizin (MDC), Berlin, Germany

<sup>2</sup>NeuroCure Cluster of Excellence, Charité, Berlin, Germany

<sup>§</sup>Graduate student at the Freie Universität Berlin

\* Corresponding author: [Jentsch@fmp-berlin.de](mailto:Jentsch@fmp-berlin.de)

**Canonical olfactory signal transduction involves the activation of cAMP-activated cation channels that depolarize the cilia of receptor neurons and raise intracellular calcium. Calcium then activates  $\text{Cl}^-$  currents that may be up to 10-fold larger than cation currents and are believed to powerfully amplify the response. We now unambiguously identified *Ano2* (Anoctamin2, TMEM16B) as the long-sought ciliary  $\text{Ca}^{++}$ -activated  $\text{Cl}^-$  channel of olfactory receptor neurons. *Ano2* is expressed in the main olfactory epithelium (MOE) and in the vomeronasal organ (VNO) that additionally expresses the related *Ano1* channel. Disruption of *Ano2* in mice virtually abolished  $\text{Ca}^{++}$ -activated  $\text{Cl}^-$  currents in the MOE and VNO. Surprisingly, *Ano2* disruption reduced fluid phase electroolfactogram responses by only ~40%, did not change air phase electroolfactograms, and did not reduce performance in olfactory behavioral tasks. In contrast to the current view, cyclic nucleotide-gated cation channels do not need a boost by  $\text{Cl}^-$  channels to achieve near-physiological levels of olfaction.**

Olfaction in mammals involves the binding of odorants to a subset of a very large number of different G-protein coupled receptors that are present in the cilia of olfactory sensory neurons (OSNs)<sup>1</sup>. These neurons are predominantly found in the main olfactory epithelium which senses and discriminates myriads of volatile compounds. In the mouse, the nose contains additional, apparently more specialized olfactory organs like the septal organ of Masera or the vomeronasal organ<sup>2</sup>. Sensory neurons in the latter organ are morphologically distinct and use odorant receptors and signal transduction cascades that differ from those found in the MOE.

In the canonical OSN signal transduction pathway, odorant binding to the receptor locally increases cytosolic cAMP levels through activation of the olfactory G-protein  $G_{\text{olf}}$  and adenylate cyclase type III<sup>1,2</sup>. cAMP then opens heteromeric cyclic-nucleotide gated (CNG) cation channels<sup>3</sup>. The resulting influx of  $\text{Na}^+$  and  $\text{Ca}^{++}$  depolarizes the plasma membrane and raises the cytosolic  $\text{Ca}^{++}$  concentration ( $[\text{Ca}^{++}]_i$ ), thereby activating  $\text{Ca}^{++}$ -activated  $\text{Cl}^-$  channels<sup>1,4-10</sup>. All

these components of the signal transduction cascade are localized to sensory cilia which are embedded in the mucus covering the MOE. These cilia provide a large interaction surface for odorants and their small diameter facilitates large local increases in cytosolic cAMP and  $[Ca^{++}]$ .

There has been broad consensus that  $Ca^{++}$ -activated  $Cl^-$  channels powerfully amplify olfactory signal transduction<sup>1,4-10</sup>. These channels are thought to mediate an outward flow of  $Cl^-$  which generates a depolarizing current that in rodents is 5- to 10-fold larger than currents through CNG channels<sup>8,11,12</sup>. A prerequisite for  $Cl^-$  efflux is an inside-out electrochemical  $Cl^-$ -gradient. It is believed that cytosolic chloride concentration of OSNs is raised by the  $Na^+K^+2Cl^-$  cotransporter *Nkcc1*<sup>9,10,13</sup> and that  $[Cl^-]$  in the mucus surrounding cilia is low<sup>14,15</sup>. However, mucosal ion concentrations are difficult to measure *in vivo* and *Nkcc1* knock-out (KO) mice display attenuated electroolfactograms<sup>11,16</sup>, but normal olfactory sensitivity<sup>17</sup>.

To investigate the role of  $Ca^{++}$ -activated  $Cl^-$  channels in olfaction, we disrupted *Ano2* in mice. *Ano2* is a member of the *Anoctamin* (*Tmem16*) gene family which encodes several  $Ca^{++}$ -activated  $Cl^-$  channels<sup>18-20</sup>. Agreeing with recent results<sup>13,21-23</sup>, our KO-controlled immunolabeling showed *Ano2* expression in cilia of OSNs in the MOE, in microvilli of VNO sensory neurons and in synapses of photoreceptors. Additionally, we found *Ano2* in the olfactory bulb. *Ano1* expression overlaps with *Ano2* in the VNO and the retina, but not in the MOE. Patch-clamp analysis showed that  $Ca^{++}$ -activated  $Cl^-$  currents were undetectable in *Ano2*<sup>-/-</sup> OSNs. Unexpectedly, however, electroolfactograms of *Ano2*<sup>-/-</sup> mice were reduced only by up to ~40% and *Ano2*<sup>-/-</sup> mice were able to smell normally. Our work calls for a revision of the current view that  $Ca^{++}$ -activated  $Cl^-$  channels play a crucial role in mammalian olfaction.

## RESULTS

### Disruption of *Ano2* and *Ano2* expression pattern

We generated *Ano2*<sup>-/-</sup> mice by flanking exon 12 with loxP sites and crossing these mice with Cre-recombinase expressing *deleter* mice<sup>24</sup> (**Supplementary Fig. 1a,b**). The ~160 kDa band representing the *Ano2* protein in *Ano2*<sup>+/+</sup> (wild-type, WT) olfactory epithelium was absent from *Ano2*<sup>-/-</sup> tissue (**Fig. 1a**). Our N-terminal antibody did not detect a truncated protein in *Ano2*<sup>-/-</sup> tissue, suggesting nonsense-mediated mRNA decay, instability of the truncated protein, or both. *Ano2*<sup>-/-</sup> mice were born at Mendelian ratio, grew, mated, and survived normally and lacked an immediately apparent phenotype.

Consistent with previous data<sup>21-23</sup>, Western blots indicated that *Ano2* is most highly expressed in olfactory epithelium (MOE and VNO) and eye (**Fig. 1a,b**). *Ano2* was expressed at much lower levels in brain, with highest expression in the olfactory bulb and signals near the detection limit in midbrain and brainstem (**Fig. 1b**). No expression was detected in cortex, cerebellum and trigeminal nerve. The differences in apparent sizes of *Ano2* among various tissues are largely owed to a higher degree of glycosylation in olfactory tissues (**Supplementary Fig. 2**). Immunolabeling revealed that *Ano2* is expressed on the apical surface of both the MOE and the VNO (**Fig. 2a**). In the MOE, it co-localized with the cilia marker protein acetylated tubulin (**Fig. 2b**) and the *Cnga2* subunit of the olfactory CNG channel<sup>3,25,26</sup> (**Fig. 2c**). *Ano2* staining was specific as no signal was observed in *Ano2*<sup>-/-</sup> tissue (**Fig. 2c**).

*Ano2* was also detected in vomeronasal sensory neurons (VSNs), where it co-localized with the closely related *Ano1* Cl<sup>-</sup> channel in sensory protrusions (**Fig. 3a**). In the MOE, however, *Ano1* could not be detected in olfactory sensory neurons (**Fig. 3b,c**), but in Bowman's glands (not shown). Likewise *Ano1* was found in apical membranes of nasal glands (**Fig. 3b,d**) and non-ciliated cells of the respiratory epithelium (**Fig. 3b-d**), consistent with a role in salt secretion as in other epithelia<sup>18,27,28</sup>.

We detected the Ano2 protein also on OSN axons that converge on glomeruli in the olfactory bulb (**Fig. 4a,b**). In the eye, our KO-controlled staining confirmed the presence of Ano2 in the outer plexiform layer of the retina<sup>22</sup> (**Supplementary Fig. 3a**). Ano2 co-localized with the PSD-95 adaptor protein (**Supplementary Fig. 3b**) and the Ca<sup>++</sup>-ATPase PMCA (**Supplementary Fig. 3c**) in presynaptic structures of photoreceptors, where these proteins form a complex together with MPP4<sup>22</sup>. Whereas Ano2 is lost from photoreceptors of *Mpp4*<sup>-/-</sup> mice<sup>22</sup>, loss of Ano2 affected neither PSD-95 nor PMCA expression (**Supplementary Fig. 3b,c**). Ano1 antibodies labeled the same Ano2-positive presynaptic structures (**Supplementary Fig. 3a**).

### **No change of key proteins and axonal convergence**

Neither immunohistochemistry (**Fig. 3a**) nor immunoblots (**Supplementary Fig. 4a**) indicated an upregulation of Ano1 in the VNO or MOE of *Ano2*<sup>-/-</sup> mice. Consistent with the normal morphology of both olfactory organs in *Ano2*<sup>-/-</sup> mice (**Figs. 2c, 3a**), expression levels of the olfactory marker protein OMP<sup>29</sup> were unchanged (**Supplementary Fig. 4b**). *Ano2* disruption neither changed the expression of the downstream target of G<sub>olf</sub>, adenylylase cyclase III (**Supplementary Fig. 4c,f**), nor of the cAMP-activated cation channel subunit Cnga2 (**Fig. 2c, Supplementary Fig. 4d**). Levels of Nkcc1, Ano6, Ano8, and Ano10 were also unaltered (**Supplementary Fig. 4f**).

Immunohistochemistry (**Fig. 4a**) and immunoblots (**Supplementary Fig. 4e**) revealed no change in the amount of tyrosine hydroxylase in the olfactory bulb, either. The expression of this enzyme depends on neuronal activity and was severely reduced in the olfactory bulb of anosmic *Cnga2*<sup>-/-</sup> mice<sup>30</sup>. OSN axon coalescence on glomeruli is perturbed in mice lacking functional CNG channels<sup>31</sup> or the adenylylase cyclase<sup>32</sup>. No obvious change in axonal convergence could be detected for OSNs expressing either the P2 or M72 receptor<sup>31</sup> (**Fig. 4c–e**). These observations suggest that olfaction is not grossly impaired in *Ano2*<sup>-/-</sup> mice and that intrinsic OSN activity is not changed to a degree that changes the olfactory map.

### **Ca<sup>++</sup>-activated Cl<sup>-</sup> currents are absent from *Ano2*<sup>-/-</sup> OSNs**

Whole-cell patch-clamp analysis of OSNs from the MOE *in situ* under conditions that largely suppress cation currents revealed Ca<sup>++</sup>-activated Cl<sup>-</sup> currents (**Fig. 5d,f,g,i**) that were not observed in the absence of intracellular Ca<sup>++</sup> (**Fig. 5a–c**). These currents showed typical time-dependence and outward rectification at 1.5 μM (**Fig. 5d,f**), but not at 13 μM free Ca<sup>++</sup> (**Fig. 5g,i**) similar to Ca<sup>++</sup>-activated Cl<sup>-</sup> currents reported for heterologously expressed Ano1 and Ano2<sup>20-22,33,34</sup> and for frog OSNs<sup>7</sup>. These Cl<sup>-</sup> currents were undetectable in *Ano2*<sup>-/-</sup> OSNs (**Fig. 5e,f,h,i**). To exclude that transient Ca<sup>++</sup>-activated Cl<sup>-</sup> currents remain in *Ano2*<sup>-/-</sup> OSNs, we used flash photolysis of caged Ca<sup>++</sup> with isolated receptor neurons. Like observed previously<sup>12,35</sup>, *Ano2*<sup>+/+</sup> neurons responded with large, rapidly activating, transient currents that reversed close to the Cl<sup>-</sup>-equilibrium potential (**Fig. 6a,c**). *Ano2*<sup>-/-</sup> OSNs responded with >10-fold smaller currents that reversed close to the K<sup>+</sup>-equilibrium potential. Flash release of 8-Br-cAMP elicited large currents in *Ano2*<sup>+/+</sup>, but not in *Ano2*<sup>-/-</sup> OSNs (**Fig. 6b**). Currents remaining in *Ano2*<sup>-/-</sup> neurons most likely represent cation currents through CNG channels<sup>12</sup>. We conclude that Ca<sup>++</sup>-activated Cl<sup>-</sup>-currents of OSNs are mediated by Ano2.

In the VNO, both *Ano2*<sup>+/+</sup> and *Ano2*<sup>-/-</sup> VSNs had low background currents in the absence of intracellular Ca<sup>++</sup> (**Fig. 5j–l**). In *Ano2*<sup>+/+</sup> VSNs 1.5 μM [Ca<sup>++</sup>]<sub>i</sub> elicited Cl<sup>-</sup> currents with an outwardly rectifying, time-dependent component (**Fig. 5l,m**). Currents of most *Ano2*<sup>-/-</sup> VSNs were undistinguishable from those observed without Ca<sup>++</sup> (**Fig. 5n**), but a few cells showed up to 2-fold larger currents. Averaged I/V curves revealed that Ca<sup>++</sup>-activated Cl<sup>-</sup> currents of VSNs depend predominantly on Ano2 (**Fig. 5l**). Although Ano1 is expressed in the VNO (**Fig. 3a**), its contribution to VSN currents seems minor.

### **Disruption of Ano2 moderately reduces electroolfactograms**

The role of Ano2 in the MOE response to odorants was investigated by electroolfactograms (EOGs) *ex vivo* (**Fig. 7a–g**). In fluid phase EOGs the surface of turbinates was continuously superfused with Ringer solution and an odorant

cocktail was applied (**Fig. 7a,b**). The superfusate could be switched to a solution containing niflumic acid (NFA). NFA has been widely used to block  $\text{Ca}^{++}$ -activated  $\text{Cl}^-$  channels in OSNs and other cells<sup>4,6,9,11,16,34,36,37</sup> and inhibits both *Ano1* and *Ano2*<sup>18,20,21,33,34</sup>. The response to odorants was reduced by roughly 40% in *Ano2*<sup>-/-</sup> EOGs compared to WT (**Fig. 7e**). Similar reductions of EOG amplitudes by *Ano2* disruption were observed when adenylate cyclase was directly activated by forskolin (**Fig. 7c–e**), or with single odorants (**Fig. 7f**). As expected, NFA-insensitive voltage excursions were similar in both genotypes (**Fig. 7e**). Importantly, NFA also inhibited odorant-induced responses in *Ano2*<sup>-/-</sup> epithelia (**Fig. 7b,e**). Comparison between *Ano2*<sup>+/+</sup> and *Ano2*<sup>-/-</sup> mice revealed that only ~60% of the response to NFA was owed to an inhibition of *Ano2*. Hence previous studies<sup>9,11,37</sup> may have overestimated the role of  $\text{Ca}^{++}$ -activated  $\text{Cl}^-$  channels in olfaction.

In air phase EOGs the surfaces of turbinates were exposed to water-saturated air and odorant or vehicle was applied by an air puff. In this configuration mucosal ion concentrations more closely match physiological levels. Contrasting with fluid phase EOGs (**Fig. 7a–f**), no significant differences between the genotypes were detected (**Fig. 7g**).

With appropriate driving forces, apical  $\text{Cl}^-$  channels may change mucosal ion composition, similar to the proposed role of *Ano1* in secretory epithelia<sup>18,27,28</sup>. However,  $\text{Cl}^-$ -sensitive microelectrode measurements showed no difference in mucosal  $[\text{Cl}^-]$  between the genotypes (*Ano2*<sup>+/+</sup>:  $84.0 \pm 11.8$  mM (s.e.m., n = 6), *Ano2*<sup>-/-</sup>:  $84.4 \pm 9$  mM (s.e.m., n = 11)). These values agree with data from amphibia<sup>15</sup>.

### **No olfactory deficits detected in *Ano2*<sup>-/-</sup> mice**

Using an automated olfactometer<sup>17,30,38,39</sup>, mice were tested on an associative olfactory learning task. Mice were trained to sample two different stimuli, one of which was associated with a water reward, and to lick only in response to the rewarded odor.

Disruption of *Ano2* did not affect the performance in discrimination tests where mice learned to distinguish geraniol from the mineral oil solvent (**Fig. 8a**). By contrast, *Cnga2*<sup>-/-</sup> mice<sup>31</sup> showed a clear-cut impairment in the same test (**Fig. 8a**) as published previously<sup>25,30</sup>. Discrimination ability was neither reduced in more complex discrimination tasks such as distinguishing hexanal from octanal (**Fig. 8b**), or differentiating between a (-)-limonene and an enantiomeric mixture of equal parts of (+)- and (-)-limonene (**Fig. 8c**). Discrimination between 0.4% hexanal/0.6% octanal and 0.6% hexanal/0.4% octanal was even more difficult, as evident from the larger number of trials needed to distinguish both mixtures (**Fig. 8d**). Even in this task *Ano2*<sup>-/-</sup> mice performed like WT. Using successive dilutions of geraniol we tested whether the loss of *Ano2* affected odor sensitivity. With either genotype, odor detection dropped sharply when the dilution reached 10<sup>-7</sup> (**Fig. 8e**). We conclude that Ca<sup>++</sup>-activated Cl<sup>-</sup> channels are not essential for olfaction.

## DISCUSSION

Ca<sup>++</sup>-activated Cl<sup>-</sup> channels are prominently expressed in olfactory sensory neurons. In freshwater animals, where ion gradients preclude a depolarizing influx of monovalent cations, Cl<sup>-</sup> efflux may generate almost all of the receptor current<sup>5,40</sup>. By contrast, the cation concentration in the mucus surrounding olfactory cilia in mammals<sup>14,15</sup> allows for a sizeable depolarization when CNG channels open upon an odorant-induced rise in cAMP. After first publications had shown that Ca<sup>++</sup>-activated Cl<sup>-</sup> currents could powerfully amplify olfactory receptor currents<sup>4-7</sup>, this concept has received support from many groups. Experiments with isolated receptor neurons<sup>4-6,8</sup> showed that up to 80-90% of the receptor current is carried by Cl<sup>-</sup>. An important role for Cl<sup>-</sup> in olfaction was also inferred from electroolfactograms<sup>11,16,37</sup>. However, since the molecular identity of the olfactory Ca<sup>++</sup>-activated Cl<sup>-</sup> channel has remained elusive<sup>35</sup>, the role of Cl<sup>-</sup> channels in olfaction could not be tested directly.

Olfactory cilia express Bestrophin-2<sup>41</sup> and Ano2<sup>13,21</sup>, which were both hypothesized to mediate ciliary Ca<sup>++</sup>-activated Cl<sup>-</sup> currents. A role of Bestrophin-2 has recently been excluded by normal Cl<sup>-</sup> currents in *Best2*<sup>-/-</sup> OSNs<sup>35</sup>. The present work unambiguously identifies Ano2 as the long-sought olfactory Ca<sup>++</sup>-activated Cl<sup>-</sup> channel, or at least as an essential component thereof. Although Ano1 is expressed in the VNO, its contribution to Ca<sup>++</sup>-activated Cl<sup>-</sup> currents in VSNs seems minor.

Surprisingly, *Ano2*<sup>-/-</sup> mice had no detectable impairment of olfaction. This is not owed to a compensatory upregulation of other Ca<sup>++</sup>-activated Cl<sup>-</sup> channels or of the cyclic-nucleotide-gated channel. The normal growth and survival of newborn *Ano2*<sup>-/-</sup> mice already indicated that they could smell the teats of their mothers. Near-normal olfaction was indirectly suggested by unaltered tyrosine hydroxylase expression in the olfactory bulb, apparently normal axonal coalescence on glomeruli in the olfactory bulb, and was confirmed by quantitative olfactometry. In contrast to *Ano2*<sup>-/-</sup> mice, *Cnga2*<sup>-/-</sup> mice display severely impaired olfaction (ref. 25,30 and present work). We conclude that CNG-mediated cation currents do not need an additional boost by anion currents for near-physiological levels of olfactory sensitivity.

Whereas fluid phase electroolfactograms revealed a significant difference between the genotypes, the ~40% reduction of *Ano2*<sup>-/-</sup> EOG amplitudes is much less than expected from the published 80-90% contribution of Cl<sup>-</sup> to OSN receptor currents<sup>8,11,12</sup>. The contribution of Ca<sup>++</sup>-activated Cl<sup>-</sup> channels was often estimated from the inhibition by NFA<sup>11,37</sup>, but this compound also modulates several other ion channels (e.g. ref. 42,43). The attenuation of *Ano2*<sup>-/-</sup> EOGs by NFA now demonstrates that NFA also affects MOE targets other than Ca<sup>++</sup>-activated Cl<sup>-</sup> channels. Hence, previous studies based on NFA-inhibition<sup>11,37</sup> have overestimated the role of Ca<sup>++</sup>-activated Cl<sup>-</sup> channels. These channels might contribute only about 40% to receptor currents *in vivo*.

The ~40% reduction of fluid phase EOG in *Ano2*<sup>-/-</sup> mice fits well to the ~39% to ~57% reduction of EOG amplitudes in *Nkcc1*<sup>-/-</sup> mice<sup>11,16</sup>. The Na<sup>+</sup>K<sup>+</sup>2Cl<sup>-</sup> cotransporter *Nkcc1* may accumulate Cl<sup>-</sup> into OSNs<sup>9-11,13</sup>, a prerequisite for

depolarizing  $\text{Cl}^-$  currents. Based on the NFA-block of *Nkcc1*<sup>-/-</sup> EOG responses, the authors<sup>11</sup> concluded that a substantial depolarizing  $\text{Cl}^-$  current remained in *Nkcc1*<sup>-/-</sup> OSNs and proposed that other transporters contribute to intracellular  $\text{Cl}^-$ -accumulation<sup>11,16</sup>. The sizeable unspecific component of NFA-inhibition observed here, however, suggests that their results<sup>11,16</sup> are consistent with *Nkcc1* being the main  $\text{Cl}^-$  accumulator of OSNs. In *Nkcc1*<sup>-/-</sup> mice, intraciliary  $[\text{Cl}^-]$  is then expected to be close to equilibrium and opening of *Ano2* channels should shunt rather than amplify receptor currents. Such a shunting inhibition may explain the larger decrease of EOG amplitudes in *Nkcc1*<sup>-/-</sup> mice compared to *Ano2*<sup>-/-</sup> mice.

How can the roughly 40% reduction of fluid phase EOG amplitude, and almost no reduction of air phase EOGs, be reconciled with previous studies that reported a large, up to 80-90% contribution of  $\text{Cl}^-$  to receptor currents? Many of those studies used isolated receptor neurons patch-clamped at the cell body<sup>1,4-8,12</sup>. Also our experiments on isolated OSNs suggest a ~90% contribution of *Ano2* to cAMP-induced currents. The disruption of tight junctions during isolation of OSNs may allow ciliary *Ano2* channels to spread to the cell body where their electrical accessibility is much better<sup>10</sup>. The length (20–30  $\mu\text{m}$ ) and small diameter (0.1  $\mu\text{m}$ ) of cilia implies that channels in their distal part contribute little to voltage changes at the cell body, in particular when ciliary membrane conductance is high during signal transduction<sup>44</sup>.

Another important consequence of ciliary geometry is the rapid dissipation of ion gradients. Taking into account ion concentrations measured in the mucus and the dendritic knob (as surrogate for cilia)<sup>10,14,15</sup>,  $\text{Cl}^-$  gradients across the ciliary membrane should dissipate more easily than those for  $\text{Na}^+$  or  $\text{Ca}^{++}$  which carry depolarizing currents through CNG channels. *Nkcc1* is thought to rapidly replenish ciliary  $\text{Cl}^-$  that exits through anion channels during signal transduction<sup>10,13</sup>. Under physiological conditions, the driving force for *Nkcc1*-mediated ciliary  $\text{Cl}^-$  uptake is small<sup>10</sup> owing to rather low mucosal  $[\text{Na}^+]$  (55 or 85 mM<sup>14,15</sup>) and  $[\text{Cl}^-]$  (55 or 93 mM<sup>14,15</sup>; 84 mM (this work)). The driving force for  $\text{Cl}^-$  uptake is larger in extracellular Ringer-type solutions (> 140 mM NaCl) that were

used with isolated OSNs. Hence more efficient ciliary  $\text{Cl}^-$  replenishment from Ringer solution than from mucus may lead to larger signal amplification by  $\text{Cl}^-$  channels in isolated OSNs and in fluid phase EOGs than observed in air phase EOGs and olfaction *in vivo*.

If the 40% reduction in  $Ano2^{-/-}$  fluid phase EOG amplitude translates into a similar reduction of action potential firing *in vivo*, our olfactory tests may not be sensitive enough to detect ensuing moderate changes in olfaction thresholds. On the other hand, air phase EOGs, which more closely reflect the physiological situation, were not significantly impaired by  $Ano2$  disruption, suggesting that the olfactory information conveyed to the brain might be nearly unchanged. Notably, there are patients with van Willebrand syndrome who carry a large genomic deletion<sup>45</sup> that includes  $ANO2$  ( $TMEM16B$ ). Consistent with the present work, no impairment of olfaction was reported. The expression of  $\text{Ca}^{++}$ -activated  $\text{Cl}^-$  channels in mammalian OSNs may be an evolutionary vestige from freshwater animals<sup>5,40</sup>, or may serve also in mammals to allow consistent olfaction in face of variations of extracellular ion concentrations.  $Ano2$  may also affect the mucosal fluid film in face of strong odors, although we found unaltered mucosal  $\text{Cl}^-$  concentration under steady state. Alternatively,  $Ano2$  might confer a slight increase in olfactory sensitivity that provides an evolutionary advantage. Clearly, however,  $\text{Ca}^{++}$ -activated  $\text{Cl}^-$  channels are dispensable for near-normal olfaction and the importance of these channels for olfactory signal amplification has been overestimated.

## **ACKNOWLEDGEMENTS**

We thank Peter Mombaerts for generously providing *Cnga2*<sup>-/-</sup>, P2-IRES-tauLacZ and M72-IRES-tauLacZ mice, Volker Hagen for caged 8-Br-cAMP, Ibrahim Zarour and Uwe Heinemann for help with ion-selective microelectrodes, Sabrina Jabs and Lilia Leisle for help with flash photolysis, Peter Mombaerts and Björn Schroeder for helpful discussions, and Nicole Krönke and Franziska Binder for technical assistance. This work was supported, in part, by the Prix Louis-Jeantet de Médecine to TJJ.

## **AUTHOR CONTRIBUTIONS**

GMB generated *Ano2*<sup>-/-</sup> mice and Ano2 antibodies, designed, performed and evaluated expression analysis and immunohistochemistry, olfactometry and mouse behavioral studies, and wrote the paper. BP designed, performed and evaluated patch-clamp analysis, electroolfactogram and ion-selective microelectrode measurements, and wrote the paper. BP and PF designed, performed and evaluated flash-photolysis experiments. TJJ initiated the project, designed and evaluated experiments, and wrote the paper.

## FIGURE LEGENDS

**Figure 1** Immunoblot analysis of An2 expression. (a) An2 expression in the main olfactory epithelium (MOE), vomeronasal organ (VNO) and eye of *Ano2*<sup>+/+</sup>, but not of *Ano2*<sup>-/-</sup> mice. Protein loaded: 16 µg (MOE) and 100 µg (other lanes). (b) An2 is detected in lower amounts in olfactory bulb, midbrain and brainstem, but not in cortex, cerebellum and trigeminus. α-tubulin serves as loading control. Protein loaded: MOE, 1.6 µg; eye, 10 µg; other lanes, 50 µg. The sharp ~140 kDa band remaining in *Ano2*<sup>-/-</sup> tissue is non-specific. The broad band (\*) in midbrain and brain stem represents An2 since it is absent from *Ano2*<sup>-/-</sup> tissue and runs at a similar size as in the retina.

**Figure 2** An2 localizes to sensory protrusions in olfactory epithelia. (a) Coronal view of the posterior part of the nasal cavity stained for An2 (antibody rbAno2\_N3-3). An2 localized to the surface of the main olfactory epithelium (MOE) and the vomeronasal organ (VNO), but not to the respiratory epithelium (RE). Nuclei (blue) are only shown in the right half of the picture. Scale bar, 500 µm. (b) Confocal images of the transition region from MOE to RE shows An2 expression exclusively in OSNs where it co-localizes with acetylated tubulin. (c) Co-localization of An2 and Cnga2 in the MOE. Merged images with nuclei labeled in blue are superimposed on transmission light pictures. Scale bar, 20 µm. Arrowheads mark transition from MOE to RE.

**Figure 3** An2 and An1 are co-expressed in the VNO but not in the MOE. (a) Confocal image of the VNO co-labeled for An2 (antibody gpAno2\_C1-3) and An1 shows that both proteins are expressed in sensory protrusions of VSNs. Staining of *Ano2*<sup>-/-</sup> VNO confirms anti-Ano2 antibody specificity and reveals normal expression and localization of An1. Insets in merge, higher magnification of boxed areas. (b) Overview of nasal septum stained for An1. Arrowhead marks transition between MOE and RE, and asterisk the region containing nasal glands. (c,d) An1 expression only in non-ciliated cells of the RE that lack

staining by the cilia marker acetylated tubulin (acTub) ((**d**) and high magnification insets in (**c**)). Beneath the RE, Anol is found in apical membranes of nasal gland epithelia (arrows and high magnification inset in (**d**)). Nuclei are labeled in blue and merged images are superimposed on transmission light pictures. Scale bars, 20  $\mu\text{m}$  (**a,c-d**), 50  $\mu\text{m}$  (**b**).

**Figure 4** The olfactory bulb in *Ano2*<sup>-/-</sup> and *Ano2*<sup>+/+</sup> mice. (**a**) Specific staining for Anol2 in the olfactory nerve layer and in axons entering olfactory glomeruli. Section shows part of olfactory bulb from both hemispheres, with cleft in center. Activity-dependent tyrosine hydroxylase (TH) expression in periglomerular cells is not changed in *Ano2*<sup>-/-</sup> section. (**b**) Higher magnification of glomerulus stained for Anol2 and TH. Scale bars: 200  $\mu\text{m}$  (**a**) and 50  $\mu\text{m}$  (**b**). (**c-e**) Axonal coalescence of OSNs expressing the P2 (**c,d**) or M72 (**e**) olfactory receptors on glomeruli in the olfactory bulb. Olfactory bulbs of homozygous P2-IRES-tauLacZ or M72-IRES-tauLacZ mice<sup>31</sup> with disrupted or WT *Ano2* genes were stained for LacZ. Bulbi were sectioned (**c**) or the ventral (**d**) or dorsal (**e**) side of intact bulbi were observed. No difference in coalescence was seen (Number of mouse pairs: P2, n = 9 (4-15 weeks-old), M72, n = 2 (5 weeks-old) and n = 1 (24 weeks-old)). Scale bars, 0.5 mm (**c**), 1 mm (**d,e**).

**Figure 5** Effect of *Ano2* disruption on Ca<sup>++</sup>-activated Cl<sup>-</sup>-currents in olfactory receptor neurons from the MOE (**a-i**) and the VNO (**j-l**). (**a,d,g**) Typical current traces obtained from *Ano2*<sup>+/+</sup> OSNs in the presence of nominally 0  $\mu\text{M}$ , 1.5  $\mu\text{M}$ , and 13  $\mu\text{M}$  Ca<sup>++</sup> in the recording pipette, respectively. Voltage-clamp protocol is displayed in (**a**). (**b,e,h**) Currents from *Ano2*<sup>-/-</sup> OSNs under conditions as in (**a,d,g**). (**c,f,i**) Averaged current-voltage relationships of steady-state currents with 0  $\mu\text{M}$ , 1.5  $\mu\text{M}$  and 13  $\mu\text{M}$  Ca<sup>++</sup> in the pipette, respectively. ■, WT cells, Δ, *Ano2*<sup>-/-</sup> cells. Error bars, s.e.m. Number of cells measured: (**c**) 7 WT, 7 KO; (**f**), 15 WT, 11 KO; (**i**), 14 WT, 10 KO. (**j,m**) Typical current traces of WT vomeronasal sensory neurons (VSNs) with 0  $\mu\text{M}$  Ca<sup>++</sup> (**j**) and 1.5  $\mu\text{M}$  free Ca<sup>++</sup> (**m**) in the pipette. (**k**) *Ano2*<sup>-/-</sup> VSN with 0  $\mu\text{M}$  Ca<sup>++</sup>, and (**n**) with 1.5  $\mu\text{M}$  Ca<sup>++</sup> in

the pipette. (I) Averaged current-voltage relationships from VNO receptor neurons measured with 1.5  $\mu\text{M}$   $\text{Ca}^{++}$  ( $\blacksquare$   $Ano2^{+/+}$ ,  $\square$   $Ano2^{-/-}$ ;  $n = 7$  and  $6$ , respectively) and with 0  $\mu\text{M}$   $\text{Ca}^{++}$  ( $\bullet$  WT,  $\circ$   $Ano2^{-/-}$ ;  $n = 5$  for both). Error bars, s.e.m. Voltage clamp protocol as in (a).

**Figure 6** Response of isolated olfactory receptor neurons to photoreleased  $\text{Ca}^{++}$  or 8-Br-cAMP. (a) Typical current responses to sudden  $[\text{Ca}^{++}]$ -increase of isolated OSNs from both genotypes in whole-cell patch-clamp experiments under symmetrical  $\text{Cl}^-$ . Cells were clamped to  $-50$ ,  $0$ , and  $+50$  mV. Arrows indicate flash that releases  $\text{Ca}^{++}$  from DMNP-EDTA. *Inset*, larger magnification to reveal currents remaining in  $Ano2^{-/-}$  OSNs. (b) Typical currents elicited by flash release of 8-Br-cAMP (arrows) in isolated OSNs from  $Ano2^{+/+}$  and  $Ano2^{-/-}$  mice held at  $-50$  mV. Mean amplitudes were  $-445 \pm 111$  pA and  $-43.2 \pm 9.9$  pA for  $Ano2^{+/+}$  and  $Ano2^{-/-}$  OSNs, respectively ( $\pm$  s.e.m.,  $p = 0.0016$ ). (c) Peak currents elicited by uncaging  $\text{Ca}^{++}$  as function of holding voltage, averaged from 8  $Ano2^{+/+}$  and 7  $Ano2^{-/-}$  OSNs with  $\geq 3$  mice/genotype. Error bars, s.e.m.. Significance levels (two sample t-test): \*,  $p < 0.05$ ; \*\*,  $p < 0.01$ .

**Figure 7** Electroolfactograms (EOG) from the MOE. (a) Typical fluid phase EOGs from  $Ano2^{+/+}$  and (b) from  $Ano2^{-/-}$  mice with a mixture of 17 odorants ('Mix1': isopentyl acetate, hexanal, eucalyptol, limonene, 2-heptanone, menthyl acetate, peppermint oil, eugenol, ethyl valerate, ethyl butyrate, ethyl tiglate, allyl tiglate, octanal, isobutyl propionate, acetal, hexanoic acid, 2-hexanene, 100  $\mu\text{M}$  each). Bars above traces indicate application (200 ms) of odorant mixture (lower trace) or vehicle (upper trace). Grey traces were obtained with 300  $\mu\text{M}$  NFA and black traces in Normal Ringer (NR) before and after exposure to NFA (washout). Traces were averaged from responses to 10 repeated stimuli. (c,d) Typical fluid phase EOGs evoked by 2 s application of 30  $\mu\text{M}$  forskolin (lower trace) or vehicle control (upper trace) to  $Ano2^{+/+}$  (c) and  $Ano2^{-/-}$  MOE (d). (e) Averaged EOG amplitudes from experiments as in (a–d). (f) Averaged fluid phase EOG amplitudes elicited by individual odorants at 1 mM concentration and with 1:20

diluted coyote urine. **(h)** Averaged air phase EOG amplitudes from mice of both genotypes. 'Mix1' is the same odorant mixture as in **(a)**. 'Mix2' contained 8 odorants (D-carvone, 1-heptanol, 2-methylbutyric acid, geraniol, isopentylamine, 2-hexanone, acetophenone, 1-octanal). Differences in responses between genotypes are not statistically significant. Numbers in columns, number of measurements; error bars, s.e.m. Significance levels (two sample t-test): \*,  $p < 0.05$ ; \*\*,  $p < 0.01$ ; \*\*\*,  $p < 0.001$ .

**Figure 8** *Ano2* disruption neither affected odor discrimination nor olfactory sensitivity. **(a–d)** Different discrimination tasks. Like WT littermates, *Ano2*<sup>-/-</sup> mice learned to discriminate **(a)** between 1% geraniol and the diluent mineral oil ( $n = 6$  for each genotype), **(b)** between 1% hexanal and 1% octanal ( $n = 3$  for each genotype), **(c)** between 1% (-)-limonene and an enantiomeric mixture of 0.5% (-)-limonene and 0.5% (+)-limonene ( $n = 4$  for each genotype), and **(d)** between 0.4%hexanal/0.6%octanal and 0.6%hexanal/0.4%octanal ( $n = 5$  for each genotype). Anosmic *Cnga2*<sup>-/-</sup> mice ( $n = 3$ ) could not detect 1% geraniol **(a)**. **(e)** Odor detection threshold for geraniol. Both *Ano2*<sup>-/-</sup> ( $n = 6$ ) and *Ano2*<sup>+/+</sup> littermates ( $n = 6$ ) detected geraniol and discriminated it from the diluent only down to a dilution of  $10^{-6}$ . The first data point with a geraniol dilution of  $10^{-2}$  corresponds to **(a)**. Error bars, s.e.m. There was no significant difference between *Ano2*<sup>+/+</sup> and *Ano2*<sup>-/-</sup> mice in any of these tests.

## ONLINE METHODS

**Ano2<sup>-/-</sup> mice.** An 11 kb genomic region of *Ano2* spanning exon 12 and 13 was cloned from R1 ES cells by PCR. Exon 12 was flanked with loxP sites, a FRT-flanked neomycin selection cassette inserted (**Supplementary Fig. 1**) and the construct cloned into pKO Scrambler plasmid 901 (Lexicon Genetics). The linearized targeting vector was electroporated into R1 ES cells (129/SvJ). Cells from two independent correctly targeted clones were injected into C57BL/6 blastocysts. Chimeras were crossed to C57BL/6 Cre deleter mice<sup>24</sup> for *in vivo* excision of exon 12, which eliminates part of the first extracellular loop and of the second transmembrane domain. Splicing from exon 11 to exon 13 introduces a frameshift after the first transmembrane domain. Mice were in a mixed C57BL/6-129/Svj background and littermates served as controls. Experiments used mice that were older than 4 weeks. Genotyping employed PCR with primers flanking the loxP site of the *Ano2*<sup>-</sup> allele (GGACACCCCGTACTTGAAGA and AGCACAATGCAGACCAAGTT), yielding 163 and 1051 bp products for *Ano2*<sup>-</sup> and *Ano2*<sup>+</sup> alleles, respectively.

**Mouse husbandry.** Animal care and experiments conformed to German animal protection laws and were approved by the Berlin authorities (LaGeSo). *Cnga2*<sup>-</sup> (previously called *Ocnc1*<sup>-</sup>), P2-IRES-tauLacZ and M72-IRES-tauLacZ mice were generously provided by Peter Mombaerts (MPI Biophysics Frankfurt) and have been described<sup>31</sup>.

**Generation of Ano2 antibodies.** rbAno2\_N3-3 was raised in rabbits against the N-terminal epitope <sup>128</sup>NGETGKERHGGGPGDVELG and gpAno2\_C1-3 was raised in guinea pigs against the extreme C-terminus <sup>970</sup>GDRSRRSRAASSAPSGRSQP (Pineda Antikörper-Service, Berlin). Peptides were coupled to keyhole limpet hemocyanine via C- and N-terminally added cysteins, respectively. Animals were immunized 7 times, antibodies affinity-purified from final bleeds and tested using *Ano2*<sup>-/-</sup> tissue as control.

**Immunohistochemistry.** Anesthetized mice were perfused with PBS followed by 4% paraformaldehyde (PFA) in PBS. Tissues were postfixed for 2 h (olfactory bulb) or overnight (nose, eye). 6  $\mu$ m cryosections were cut from eyes and 10  $\mu$ m cryosections from olfactory bulb. Noses were decalcified in 10% EDTA in PBS for 7 days, postfixed for 2 h, and 6  $\mu$ m paraffin sections prepared. For antigen retrieval, sections were boiled for 5 min in 10 mM citrate buffer (pH 6.0) or 10 mM Tris, 1 mM EDTA, pH 9.0, and transferred to 3% BSA in TBS with 0.2% NP-40 for blocking and antibody incubation. Antibodies used: rbAno2\_N3-3 (1:1000); gpAno2\_C1-3 (1:250); anti-TMEM16A (Ano1) rabbit polyclonal (1:100, ab53212, Abcam; its specificity had been shown using *Ano1*<sup>-/-</sup> tissue<sup>46</sup>); anti-Cnga2 goat polyclonal (1:50, CNG-2/M-20, sc-13700, Santa Cruz); anti-acetylated tubulin mouse monoclonal (1:1000, clone 6-11B-1, T7451, Sigma-Aldrich); anti-tyrosine hydroxylase mouse monoclonal (1:1000, MAB5280, Chemicon); anti-PSD-95 mouse monoclonal (1:250, clone 7E3-1B8, MA1-046, ThermoScientific); anti-PMCA mouse monoclonal (1:500, clone 5F10, MA3-914, Affinity BioReagents). Detection used secondary antibodies coupled to Alexa fluorophores (Invitrogen). Nuclei were stained with Hoechst 33258. Pictures were taken with a Zeiss LSM 510 META laser scanning microscope using a "Plan-Apochromat" 63 $\times$ /1.40 Oil DIC M27 or EC "Plan-Neofluar" 10 $\times$ /0.3 M27 objective and ZEN software.

**Determination of OSN coalescence.** P2-IRES-tauLacZ and M72-IRES-tauLacZ mice<sup>31</sup> were crossed with *Ano2*<sup>+/-</sup> mice to yield *Ano2*<sup>-/-</sup> and *Ano2*<sup>+/+</sup> littermates homozygous for these reporter lines. 5 to 24 weeks-old mice were perfused with PBS followed by 4% PFA in PBS. Brains were postfixed (20 min on ice), washed in buffer A (100 mM phosphate buffer pH 7.4, 2 mM MgCl<sub>2</sub>, 5 mM EGTA) and incubated for 30 min in buffer A with 0.02% NP-40 and 0.01% deoxycholate. LacZ staining was overnight in buffer A with 0.2% NP-40, 0.1% deoxycholate, 5 mM potassium-ferricyanide and 1 mg/ml of X-Gal at room temperature. Whole-mount stained bulbs were cryoprotected in 30% sucrose, frozen in Tissue-Tek O.C.T. compound (Sakura) and cut into 20  $\mu$ m cryostat

sections. Sections were poststained with X-Gal and counterstained with Neutral Red.

**Lysate preparation, deglycosylation and immunoblotting.** Turbinates, VNO or eyes were dissected, minced and sonicated in lysis buffer (10 mM HEPES pH 7.4, 150 mM NaCl, 5 mM EDTA, protease inhibitors, 1% SDS). Lysates from brain regions and ANO1-transfected HEK cells were prepared similarly. The ANO1 expression construct encodes a 986 aa human isoform (NM\_018043.5). For deglycosylation, lysates were incubated with 5%  $\beta$ -mercaptoethanol for 15 min at 55 °C, diluted 1:5 into deglycosylation buffer (50 mM HEPES pH 7.4, 10 mM EDTA, 0.5% Nonidet P-40, protease inhibitors) and incubated overnight at 37 °C with 1 U of N-Glycosidase F (Roche Diagnostics) per 100  $\mu$ g protein. Proteins were separated on SDS-polyacrylamide gels and transferred on polyvinylidene difluoride membranes. Antibodies and dilutions used: rbAno2\_N3-3 antibody (1:1000); anti-adenylate cyclase III rabbit polyclonal (1:2000, C-20, sc-588, Santa Cruz); anti-olfactory marker protein (OMP) goat polyclonal (1:1000, 544-10001, Wako); anti- $\alpha$ -tubulin mouse monoclonal (1:2000, clone B-5-1-2, T5168, Sigma-Aldrich); anti-Cnga2 (1:100), anti-tyrosine hydroxylase (1:5000) and anti-TMEM16A (1:250) antibodies as in immunohistochemistry. Signals were visualized by chemiluminescence (SuperSignal West, Pierce) with a PeqLab camera system and secondary antibodies coupled to horseradish peroxidase (Chemicon). Immunoblots were repeated in  $\geq 3$  independent experiments.

**Quantitative real-time PCR.** Turbinates were dissected from *Ano2*<sup>+/+</sup> and *Ano2*<sup>-/-</sup> mice (3 litter pairs, 25-27 weeks-old) and RNA isolated (RNeasy Mini Kit, Qiagen). 1  $\mu$ g RNA was subjected to desoxyribonuclease I (amplification grade, Invitrogen) digestion and transcribed into cDNA using random primers and Superscript II reverse transcriptase (Invitrogen). 20  $\mu$ l PCR reactions were set up with the Power SYBR Green PCR Master Mix (Applied Biosystems) and run in triplicates with 40 s elongation time at 60 °C. Amplification and melting curves were monitored using a StepOnePlus Real-Time PCR System and StepOne

Software (Applied Biosystems). Comparison between *Ano2*<sup>-/-</sup> and WT littermates used the Pfaffl method and  $\beta$ -actin as internal control. Primers spanned introns or exon-exon boundaries and gave products of 100 to 200 bp length. Primer pairs:

$\beta$ -actin TGTGATGGTGGGAATGGGTCAGAA,  
TGTGGTGCCAGATCTTCTCCATGT; adenylate cyclase III  
CGGCATCGAGTGTCTACGCTTC, GCCAGCGCTCCTTGTCTGACTT;  
Ano2\_ex3-4 GATGTTGAACTTGGGCCACT, CAAGAACTCTGCTTCCCTGG;  
Ano2\_ex20-21 AGGCTGTCTCATGGAGCTGT, TGCTCTGGACGTTTTGAGTG;  
Ano6 AAGAGGAACAGGCCCGGCCA, AGAAGACGGCGCTCGCACAC; Ano8  
GCGACGCGGCTGGAAGACAG, CGGCCAGTGGGAAGGCAGAG; Ano10  
AGCGGAAGTACTGTGCGAGGGT, GCAAAGGCAGCTGCTAGCGG; Nkcc1  
CTGGTGGGCTGCGTTGCTCA, GCGCTTGTGTGGAGGATCCCC.

**Tissue preparation for patch-clamping.** 6-8 weeks-old mice were sacrificed by decapitation, the MOE prepared and embedded in 4% low melting agarose in Normal Ringer (in mM: NaCl, 140; KCl, 5; glucose, 10; sodium pyruvate, 1; HEPES, 10; CaCl<sub>2</sub>, 2; MgCl<sub>2</sub>, 1; pH 7.4; osmolality, 321 mOsm kg<sup>-1</sup>). 200  $\mu$ m slices were cut perpendicular to the surface with a Leica VT1200S vibratome. The soft tissue of the VNO was embedded<sup>47</sup> in 4% low melting agarose, and cut in 200  $\mu$ m coronal slices. Slices were kept in Normal Ringer bubbled with 95% O<sub>2</sub>/ 5% CO<sub>2</sub>.

**Preparation of isolated olfactory receptor neurons.** The MOE was transferred to low Ca<sup>++</sup> Ringer (in mM: 140 NaCl, 5 KCl, 10 glucose, 1 Na-pyruvate, 1 EDTA, 1 cysteine, 10 HEPES pH 7.2) at 4 °C. After mincing, it was digested at room temperature for 20 minutes with 0.2 mg ml<sup>-1</sup> trypsin in low Ca<sup>++</sup> Ringer. The digestion was terminated with Normal Ringer containing 0.2 mg ml<sup>-1</sup> BSA, 0.2 mg ml<sup>-1</sup> leupeptin and 0.025 mg ml<sup>-1</sup> DNase I. Following gentle trituration, cells were allowed to settle on poly-L-lysine coated coverslips for 30-45 minutes at 4 °C.

**Patch-clamp analysis.** Pipettes were pulled from borosilicate glass and contained (in mM) 140 CsCl, 4 HEPES (pH 7.2), 1 EGTA, 2 Mg-ATP. Free  $[Ca^{++}]$  was adjusted according to the Maxchelator program (<http://maxchelator.stanford.edu/>) to 0, 1.5 and 13  $\mu$ M. OSNs from the MOE were patched at the cell body and sometimes at the dendritic knob, with similar results. VSNs were patch-clamped at the dendritic knob. Pipette resistances were  $\sim$  5 M $\Omega$  and 8-10 M $\Omega$  when patching OSNs or VSN dendritic knobs, respectively. Recordings were performed in the whole-cell configuration at room temperature in Normal Ringer containing 10 mM tetraethylammonium chloride using an Axon CNS MultiClamp 700B amplifier, a Digidata 1322A interface, and pClamp 10 software (Molecular Devices).

**Photorelease of caged  $Ca^{++}$  and 8-Br-cAMP.** We used [6,7-Bis(carboxymethoxy)coumarin-4-yl]methyl-8-bromoadenosine-3', 5'-cyclic monophosphate (BCMCM-caged 8-Br-cAMP), a generous gift from Volker Hagen, FMP Berlin, and DMNP-EDTA (Invitrogen). For uncaging 8-Br-cAMP, a UV flash lamp JML-C2 (Rapp OptoElektronik) was coupled to an inverted Zeiss Axiovert 200 microscope equipped with a 100 $\times$  Fluar objective.  $Ca^{++}$  was uncaged with a SP-20 UV flash lamp (Rapp OptoElektronik) coupled to an upright Olympus BX51WI microscope equipped with a 60 $\times$  LUMPlanFL objective. Isolated OSNs were patched at room temperature in the whole-cell mode. For  $Ca^{++}$  uncaging, the pipette solution contained (in mM) 140 KCl, 2 MgATP, 0.3 Na<sub>2</sub>-GTP, 10 HEPES pH 7.4, 3.5 CaCl<sub>2</sub>, and 5 DMNP-EDTA. For uncaging 8-Br-cAMP, the pipette solution contained (in mM) 145 KCl, 4 MgCl<sub>2</sub>, 1 MgATP, 0.1 Na<sub>2</sub>-GTP, 10 HEPES pH 7.4, 0.5 EGTA, and 0.1 BCMCM-caged 8-Br-cAMP. Settings were 200 V at 1 mF and 300 V at 3 mF for uncaging 8-Br-cAMP and  $Ca^{++}$ , respectively.

**Electroolfactogram (EOG) recordings.** The head was cut in the sagittal plane and the endoturbinates were exposed<sup>11,48</sup>. The lateral side of the head was immersed into 0.5% agarose gel with Normal Ringer.

In fluid phase EOGs the turbinates were continuously superfused with Normal Ringer with or without niflumic acid. The four-barrelled application pipette had two channels for continuous flow of Normal Ringer, a channel for odorant-free vehicle and for odorants. The latter two channels were connected to a Picospritzer (Toohey) to apply pressure steps. Mixtures of odorants, single odorant or forskolin (specified in legend to Fig. 7, in aqueous solution containing 0.5% DMSO) were used.

In the air phase configuration, the application tube had a channel for continuous flow of humidified 95% O<sub>2</sub>/5% CO<sub>2</sub>, and another one connected to a 15 ml bottle containing 2 ml of odorants or odorant-free vehicle and connected to a Picospritzer. 200 ms-long pressure steps were used to drive the air from the bottle to the turbinates. In both arrangements, EOGs were recorded in current clamp with an extracellular electrode filled with Ringer placed on the middle of turbinate IIb or III. EOG amplitudes from single turbinates were averaged from 10 individual sweeps and subsequently averaged from several experiments.

**Ion-sensitive microelectrodes.** Chloride-selective electrodes were fabricated<sup>49</sup> from theta-glass capillaries (Warner Instruments) with tip diameters of ~ 3 μm. Ion-selective barrels were silanized with methyltrichlorosilane in dichloromethane (Fluka/Sigma-Aldrich) and backfilled with 'Chloride ionophore I – cocktail A' (Fluka/Sigma-Aldrich). Reference barrels contained 155 mM NaCl. To exclude artifacts by Cl<sup>-</sup> diffusion, we filled them also with 40 mM NaCl/77 mM Na<sub>2</sub>SO<sub>4</sub>. No differences in measured [Cl<sup>-</sup>] were found. Measurements with either reference barrel solution were pooled. Microelectrodes connected to a differential amplifier<sup>49</sup> were lowered at a low angle onto the surface of freshly dissected turbinates. [Cl<sup>-</sup>] was determined from calibration curves before and after measurements. Measurements were discarded when these calibrations differed by > 20%.

**Olfactometry.** Behavioral assessment of odor detection and discrimination ability used a computer-controlled 8-channel liquid-dilution olfactometer (Knosys) as

described<sup>50</sup>. Mice were trained on a go/no-go operant conditioning task in which licking on a water delivery tube upon presentation of an S+ stimulus (odor 1) is associated with a water reward, but not after presentation of an S- stimulus (odor 2 or diluent). Mice able to discriminate between stimuli readily stop to answer to the S- stimulus when subjected to successive trials of S+ and S- stimuli presented in random order. Response accuracy is monitored as a measure for odor discrimination and detection ability and represents the percentage of correct answers in a block of 20 trials.

Water-deprived *Ano2*<sup>-/-</sup> mice and control littermates were trained on the BEGIN program and on a simple odor discrimination task. Tests used the D2 program with standard settings<sup>50</sup>. Chemicals were from Sigma-Aldrich/Fluka. Mice (35-41 weeks-old) were tested on 1% (-)-limonene versus 0.5% (-)/0.5% (+)-limonene (6 males, 2 females) and on geraniol dilutions (8 males, 4 females) starting with the highest concentration. Trials were 200 (down to 10<sup>-5</sup>) or 400 (10<sup>-6</sup>, 10<sup>-7</sup>) and response accuracy was calculated as mean of 3 consecutive blocks after reaching the criterion response of 90% or of the last 3 blocks in 400 trials, respectively. 14 weeks-old (4 males, 2 females) mice were used for 1% hexanal versus 1% octanal discrimination, and 6 males/4 females (50 weeks-old) for the 0.4/0.6% versus 0.6/0.4% hexanal/octanal discrimination test. 3 male *Cnga2*<sup>-/y</sup> mice (14-16 weeks old) were tested on 1% geraniol.

## REFERENCES

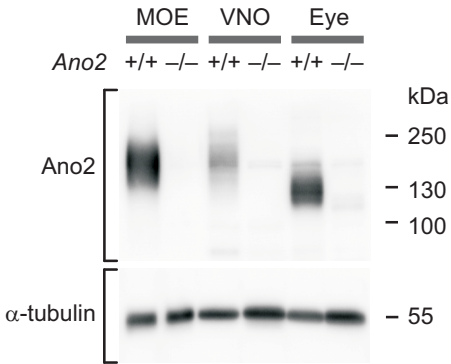
1. Kleene, S. J. The electrochemical basis of odor transduction in vertebrate olfactory cilia. *Chemical senses* **33**, 839-859 (2008).
2. Munger, S. D., Leinders-Zufall, T. & Zufall, F. Subsystem organization of the mammalian sense of smell. *Annu Rev Physiol* **71**, 115-140 (2009).
3. Bönigk, W. *et al.* The native rat olfactory cyclic nucleotide-gated channel is composed of three distinct subunits. *J Neurosci* **19**, 5332-5347 (1999).
4. Kleene, S. J. Origin of the chloride current in olfactory transduction. *Neuron* **11**, 123-132 (1993).
5. Kurahashi, T. & Yau, K. W. Co-existence of cationic and chloride components in odorant-induced current of vertebrate olfactory receptor cells. *Nature* **363**, 71-74 (1993).
6. Lowe, G. & Gold, G. H. Nonlinear amplification by calcium-dependent chloride channels in olfactory receptor cells. *Nature* **366**, 283-286 (1993).
7. Kleene, S. J. & Gesteland, R. C. Calcium-activated chloride conductance in frog olfactory cilia. *J Neurosci* **11**, 3624-3629 (1991).
8. Reisert, J., Bauer, P. J., Yau, K. W. & Frings, S. The Ca-activated Cl channel and its control in rat olfactory receptor neurons. *J Gen Physiol* **122**, 349-363 (2003).
9. Reisert, J., Lai, J., Yau, K. W. & Bradley, J. Mechanism of the excitatory Cl<sup>-</sup> response in mouse olfactory receptor neurons. *Neuron* **45**, 553-561 (2005).
10. Kaneko, H., Putzier, I., Frings, S., Kaupp, U. B. & Gensch, T. Chloride accumulation in mammalian olfactory sensory neurons. *J Neurosci* **24**, 7931-7938 (2004).
11. Nickell, W. T., Kleene, N. K., Gesteland, R. C. & Kleene, S. J. Neuronal chloride accumulation in olfactory epithelium of mice lacking NKCC1. *J Neurophysiol* **95**, 2003-2006 (2006).
12. Boccaccio, A. & Menini, A. Temporal development of cyclic nucleotide-gated and Ca<sup>2+</sup>-activated Cl<sup>-</sup> currents in isolated mouse olfactory sensory neurons. *J Neurophysiol* **98**, 153-160 (2007).
13. Hengl, T. *et al.* Molecular components of signal amplification in olfactory sensory cilia. *Proc Natl Acad Sci U S A* **107**, 6052-6057 (2010).
14. Reuter, D., Zierold, K., Schröder, W. H. & Frings, S. A depolarizing chloride current contributes to chemoelectrical transduction in olfactory sensory neurons in situ. *J Neurosci* **18**, 6623-6630 (1998).
15. Chiu, D., Nakamura, T. & Gold, G. H. Ionic composition of toad olfactory mucus measured with ion selective microelectrodes (Abstract). *Chemical senses* **13**, 677-678 (1988).
16. Nickell, W. T., Kleene, N. K. & Kleene, S. J. Mechanisms of neuronal chloride accumulation in intact mouse olfactory epithelium. *J Physiol* **583**, 1005-1020 (2007).
17. Smith, D. W., Thach, S., Marshall, E. L., Mendoza, M. G. & Kleene, S. J. Mice lacking NKCC1 have normal olfactory sensitivity. *Physiology & behavior* **93**, 44-49 (2008).

18. Yang, Y. D. *et al.* TMEM16A confers receptor-activated calcium-dependent chloride conductance. *Nature* **455**, 1210-1215 (2008).
19. Caputo, A. *et al.* TMEM16A, a membrane protein associated with calcium-dependent chloride channel activity. *Science* **322**, 590-594 (2008).
20. Schroeder, B. C., Cheng, T., Jan, Y. N. & Jan, L. Y. Expression cloning of TMEM16A as a calcium-activated chloride channel subunit. *Cell* **134**, 1019-1029 (2008).
21. Stephan, A. B. *et al.* ANO2 is the cilia calcium-activated chloride channel that may mediate olfactory amplification. *Proc Natl Acad Sci U S A* **106**, 11776-11781 (2009).
22. Stöhr, H. *et al.* TMEM16B, a novel protein with calcium-dependent chloride channel activity, associates with a presynaptic protein complex in photoreceptor terminals. *J Neurosci* **29**, 6809-6818 (2009).
23. Rasche, S. *et al.* Tmem16b is specifically expressed in the cilia of olfactory sensory neurons. *Chemical senses* **35**, 239-245 (2010).
24. Schwenk, F., Baron, U. & Rajewsky, K. A cre-transgenic mouse strain for the ubiquitous deletion of loxP-flanked gene segments including deletion in germ cells. *Nucleic Acids Res* **23**, 5080-5081 (1995).
25. Brunet, L. J., Gold, G. H. & Ngai, J. General anosmia caused by a targeted disruption of the mouse olfactory cyclic nucleotide-gated cation channel. *Neuron* **17**, 681-693 (1996).
26. Nakamura, T. & Gold, G. H. A cyclic nucleotide-gated conductance in olfactory receptor cilia. *Nature* **325**, 442-444 (1987).
27. Romanenko, V. G. *et al.* Tmem16A encodes the Ca<sup>2+</sup>-activated Cl<sup>-</sup> channel in mouse submandibular salivary gland acinar cells. *J Biol Chem* **285**, 12990-13001 (2010).
28. Rock, J. R. *et al.* Transmembrane protein 16A (TMEM16A) is a Ca<sup>2+</sup>-regulated Cl<sup>-</sup> secretory channel in mouse airways. *J Biol Chem* **284**, 14875-14880 (2009).
29. Keller, A. & Margolis, F. L. Immunological studies of the rat olfactory marker protein. *J Neurochem* **24**, 1101-1106 (1975).
30. Lin, W., Arellano, J., Slotnick, B. & Restrepo, D. Odors detected by mice deficient in cyclic nucleotide-gated channel subunit A2 stimulate the main olfactory system. *J Neurosci* **24**, 3703-3710 (2004).
31. Zheng, C., Feinstein, P., Bozza, T., Rodriguez, I. & Mombaerts, P. Peripheral olfactory projections are differentially affected in mice deficient in a cyclic nucleotide-gated channel subunit. *Neuron* **26**, 81-91 (2000).
32. Zou, D. J. *et al.* Absence of adenylyl cyclase 3 perturbs peripheral olfactory projections in mice. *J Neurosci* **27**, 6675-6683 (2007).
33. Pifferi, S., Dibattista, M. & Menini, A. TMEM16B induces chloride currents activated by calcium in mammalian cells. *Pflügers Arch* **458**, 1023-1038 (2009).
34. Sagheddu, C. *et al.* Calcium concentration jumps reveal dynamic ion selectivity of calcium-activated chloride currents in mouse olfactory sensory neurons and TMEM16B/anoctamin2-transfected HEK 293T cells. *J Physiol* **588**, 4189-4204 (2010).
35. Pifferi, S. *et al.* Calcium-activated chloride currents in olfactory sensory neurons from mice lacking bestrophin-2. *J Physiol* **587**, 4265-4279 (2009).

36. Frings, S., Reuter, D. & Kleene, S. J. Neuronal Ca<sup>2+</sup>-activated Cl<sup>-</sup> channels--homing in on an elusive channel species. *Prog Neurobiol* **60**, 247-289 (2000).
37. Pinato, G. *et al.* Electroolfactogram responses from organotypic cultures of the olfactory epithelium from postnatal mice. *Chemical senses* **33**, 397-404 (2008).
38. Bodyak, N. & Slotnick, B. Performance of mice in an automated olfactometer: odor detection, discrimination and odor memory. *Chemical senses* **24**, 637-645 (1999).
39. Kelliher, K. R., Ziesmann, J., Munger, S. D., Reed, R. R. & Zufall, F. Importance of the CNGA4 channel gene for odor discrimination and adaptation in behaving mice. *Proc Natl Acad Sci U S A* **100**, 4299-4304 (2003).
40. Kleene, S. J. & Pun, R. Y. Persistence of the olfactory receptor current in a wide variety of extracellular environments. *J Neurophysiol* **75**, 1386-1391 (1996).
41. Pifferi, S. *et al.* Bestrophin-2 is a candidate calcium-activated chloride channel involved in olfactory transduction. *Proc Natl Acad Sci U S A* **103**, 12929-12934 (2006).
42. Gribkoff, V. K. *et al.* Effects of channel modulators on cloned large-conductance calcium-activated potassium channels. *Mol Pharmacol* **50**, 206-217 (1996).
43. Vogalis, F., Hegg, C. C. & Lucero, M. T. Ionic conductances in sustentacular cells of the mouse olfactory epithelium. *J Physiol* **562**, 785-799 (2005).
44. Lindemann, B. Predicted profiles of ion concentrations in olfactory cilia in the steady state. *Biophys J* **80**, 1712-1721 (2001).
45. Schneppenheim, R. *et al.* A common 253-kb deletion involving *VWF* and *TMEM16B* in German and Italian patients with severe von Willebrand disease type 3. *J Thromb Haemost* **5**, 722-728 (2007).
46. Gomez-Pinilla, P. J. *et al.* Ano1 is a selective marker of interstitial cells of Cajal in the human and mouse gastrointestinal tract. *Am J Physiol Gastrointest Liver Physiol* **296**, G1370-1381 (2009).
47. Shimazaki, R. *et al.* Electrophysiological properties and modeling of murine vomeronasal sensory neurons in acute slice preparations. *Chemical senses* **31**, 425-435 (2006).
48. Cygnar, K. D., Stephan, A. B. & Zhao, H. Analyzing responses of mouse olfactory sensory neurons using the air-phase electroolfactogram recording. *J Vis Exp*, doi: 10.3791/1850. (2010).
49. Windmüller, O. *et al.* Ion changes in spreading ischaemia induce rat middle cerebral artery constriction in the absence of NO. *Brain* **128**, 2042-2051 (2005).
50. Slotnick, B. & Restrepo, D. Olfactometry with mice. *Current protocols in neuroscience / editorial board, Jacqueline N. Crawley ... [et al]* **Chapter 8**, Unit 8 20 (2005).

# Figure 1

**a**



**b**

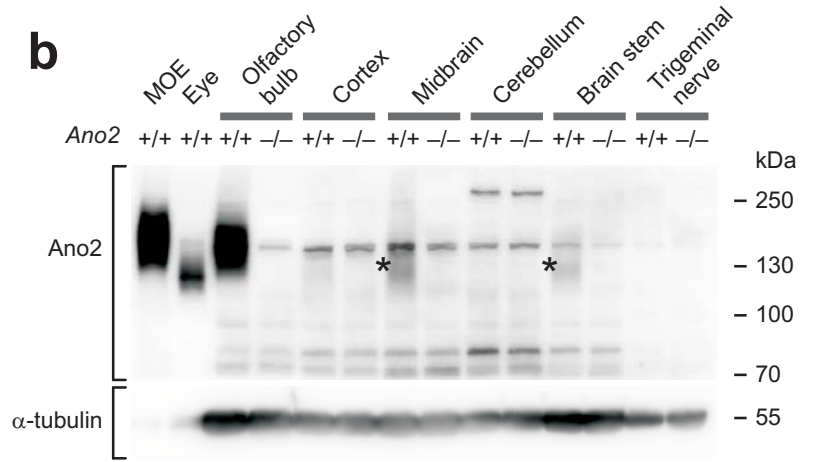


Figure 2

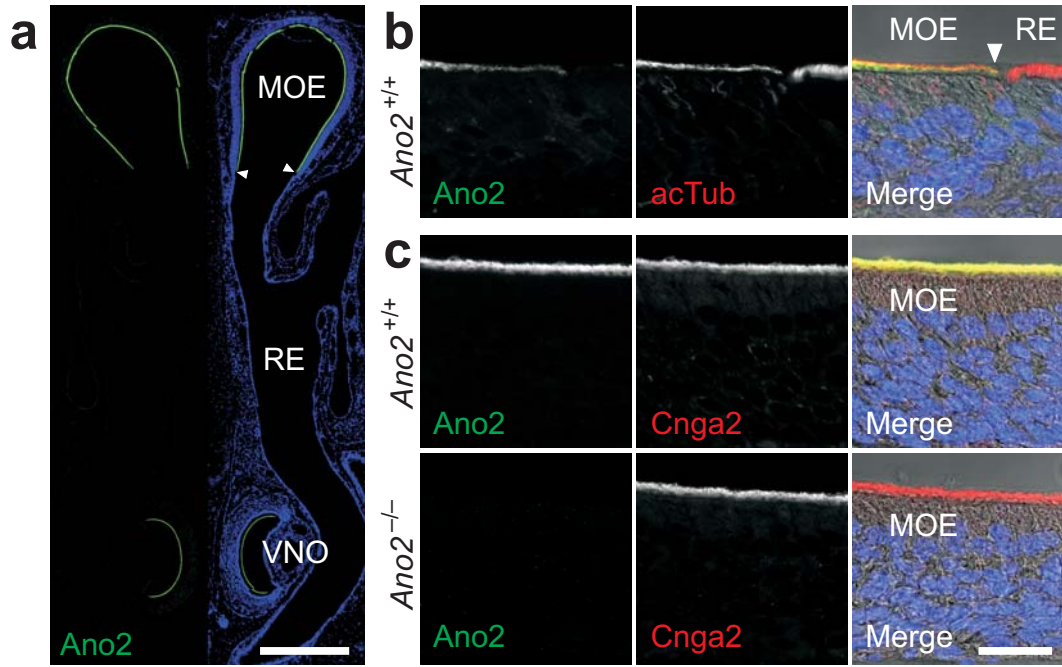


Figure 3

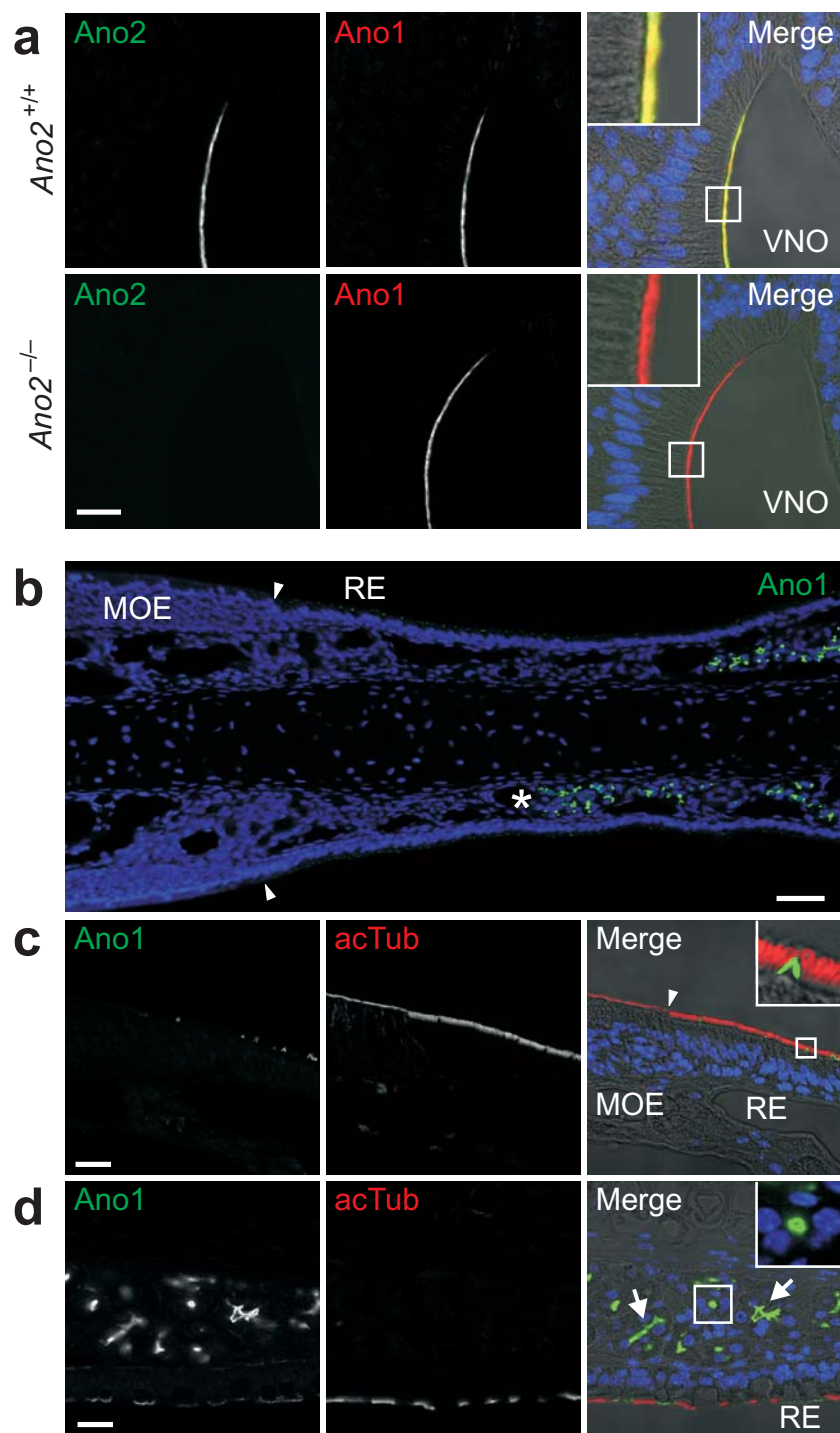
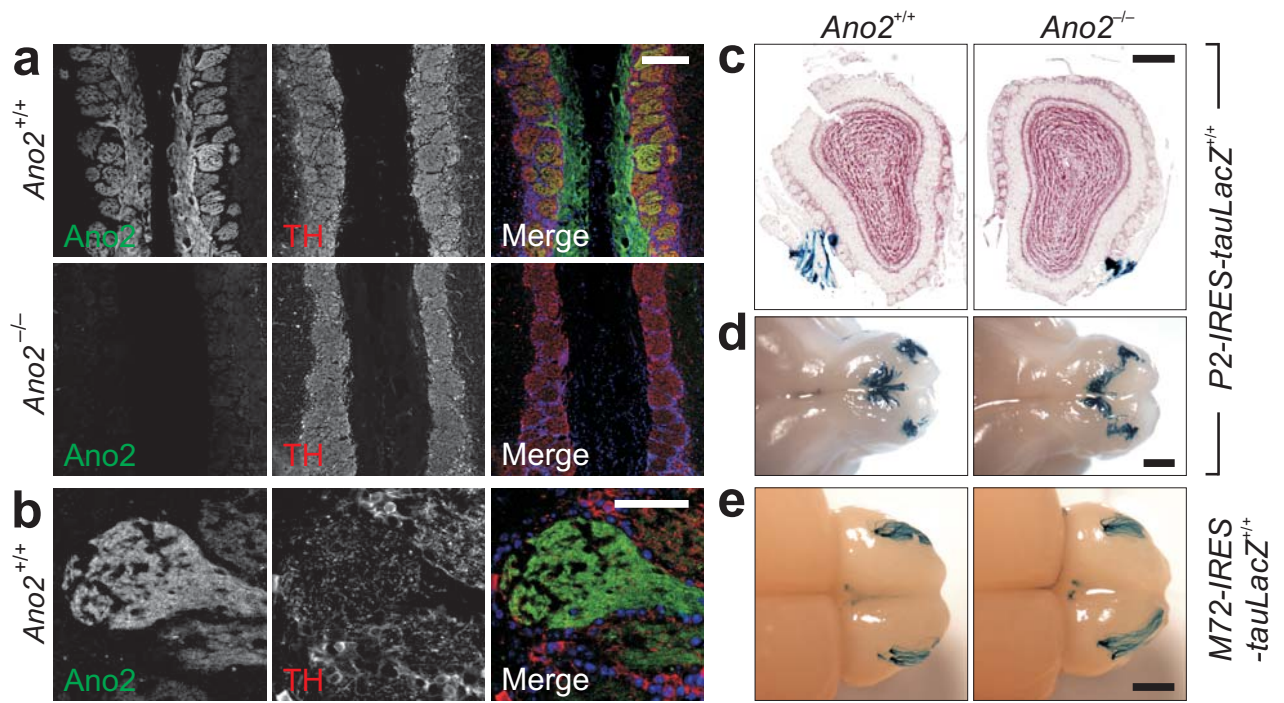
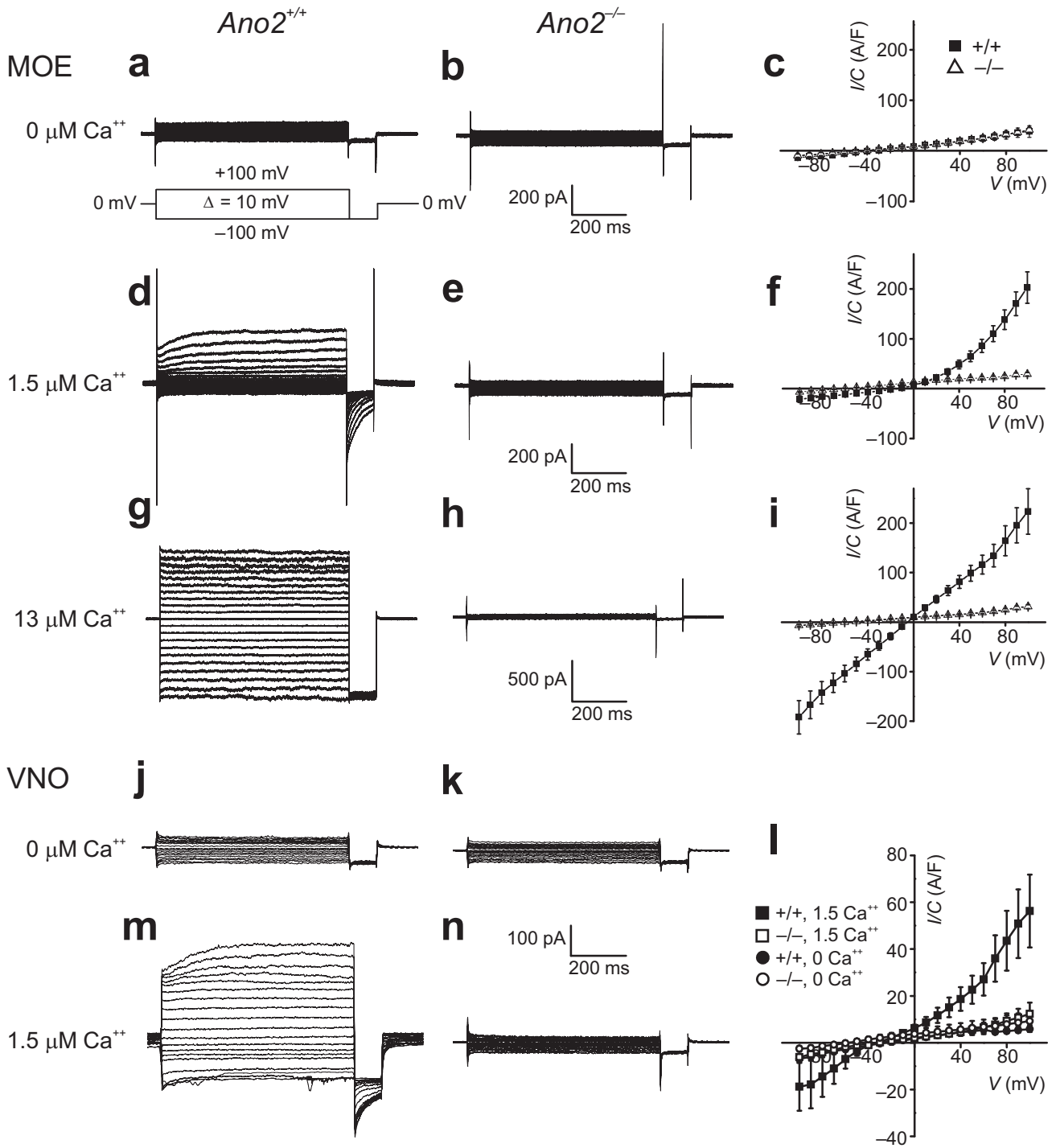


Figure 4



# Figure 5



# Figure 6

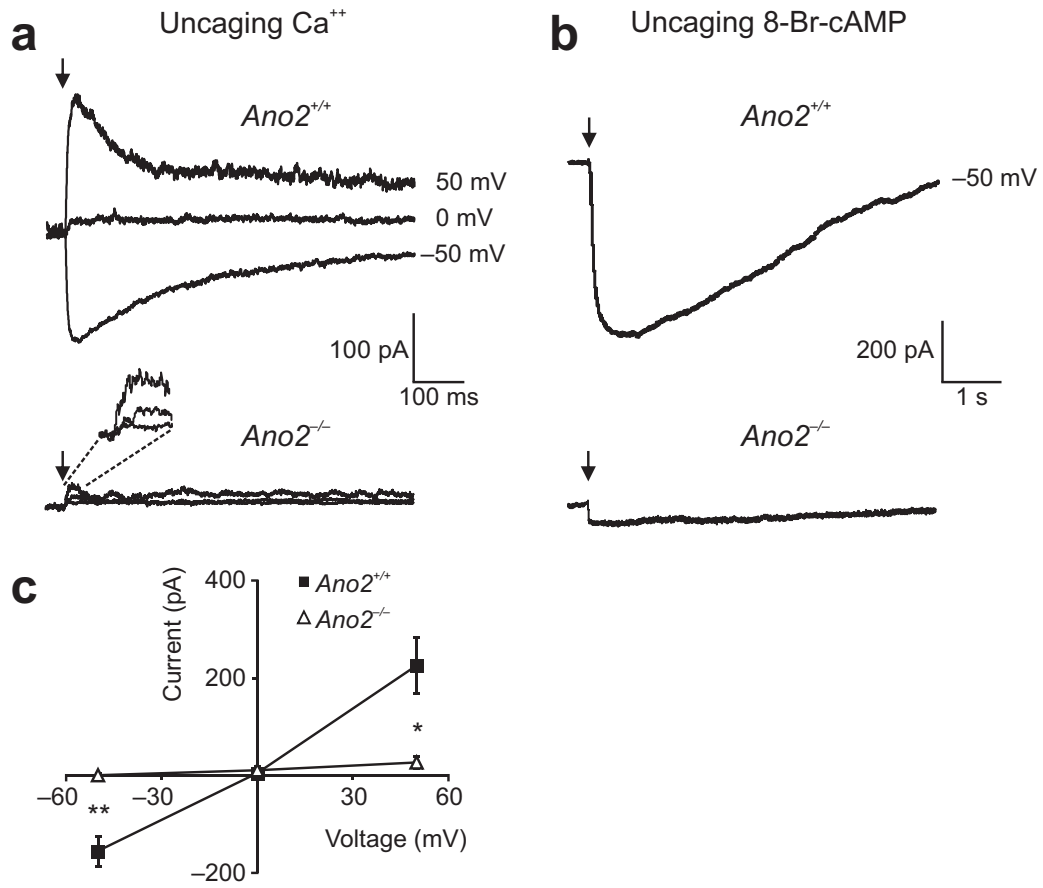


# Figure 7

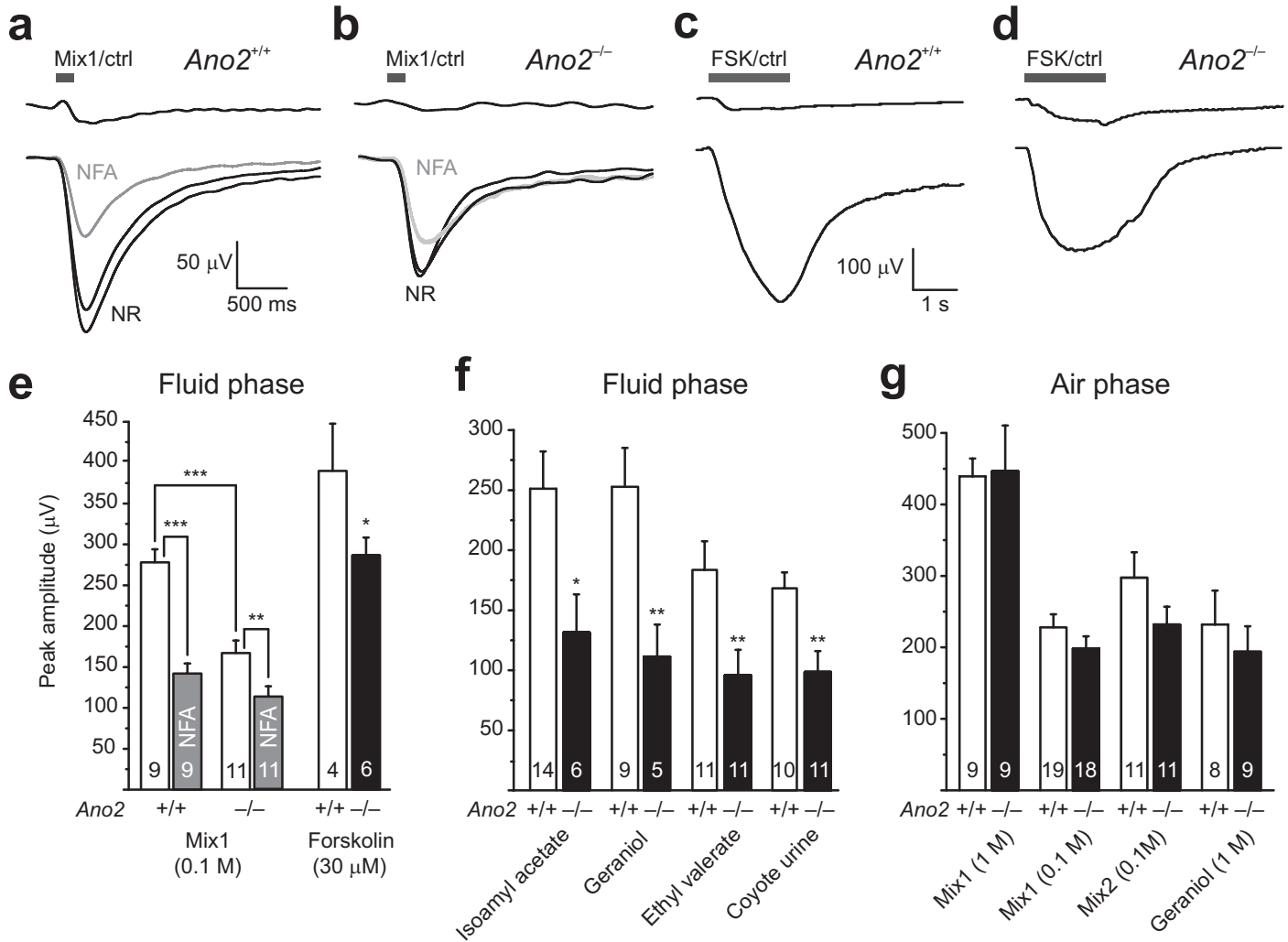


# Figure 8

